CDDpress

www.nature.com/cddis

ARTICLE OPEN

PPARγ, a key modulator of metabolic reprogramming, stemness and chemoresistance associated with retrodifferentiation in human hepatocellular carcinomas

Yoann Daniel[1], Claudine Rauch[1], Lucille Moutaux[1], Lise Desquilles[1], Tifenn Le Charpentier[1], Karim Fekir[1,2], Luis Cano[1], Daniel Catheline[1], Servane Pierre[1], Agnès Burel[3], Camille Savary[1], Catherine Ribault[1], Claude Bendavid[1,4], Bruno Clément[1], Caroline Aninat[1], Vincent Rioux[1], Orlando Musso[1], Bernard Fromenty[1], Florian Cabillic[1,4,5]✉ and Anne Corlu[1,5]✉

Human hepatocellular carcinomas (HCCs) with cancer stem cell (CSC) features are a subclass of therapeutically challenging cancers. We recently showed that retrodifferentiation of hepatic cancer cells into CSC-like cells leads to metabolic reprogramming and chemoresistance. The molecular mechanisms whereby differentiated cancer cells switch towards a CSC phenotype are poorly understood. By studying metabolic reprogramming associated with HCC cell plasticity, we identified an unsuspected role of peroxisome proliferator-activated receptor (PPAR)γ in hepatic CSC phenotype acquisition. Gene expression and metabolic analyses performed throughout the cell differentiation/retrodifferentiation process of human HepaRG and HBG-BC2 HCC cells show that metabolic reprogramming in hepatic CSCs is associated with a fragmented mitochondrial network, decreased respiration, de novo lipogenesis, and fatty acid oxidation, but increased glycolysis and lipid storage. Mitochondrial genes downregulated in HepaRG-CSCs are also downregulated in the STEM HCC subclass. While PPARα is the main isoform in differentiated hepatic cells, we find high PPARγ expression in hepatic CSCs. Accordingly, nuclear localization of PPARγ is detected in human HCC tumors, and PPARγ^{high}/PPARα^{low} expression is associated with the STEM HCC subclass and a poor outcome in human HCC cohorts. PPARγ silencing or/and inhibition of its target gene pyruvate dehydrogenase kinase 4 reactivates cell respiration, increases reactive oxygen species production and sensitizes hepatic CSCs to chemotherapy. Conversely, PPARα activation synergizes with chemotherapy to induce cell death. Targeting PPARγ, a key regulator of metabolic reprogramming and stemness in hepatic CSCs, or modulating the PPARγ/PPARα balance that finely tunes the differentiation/retrodifferentiation process in HCC deserves further investigation for anti-tumor therapy.

Cell Death and Disease (2025)16:831 ; https://doi.org/10.1038/s41419-025-07799-3

INTRODUCTION

Large-scale genome sequencing studies unravelled the molecular heterogeneity of hepatocellular carcinomas (HCCs), leading to various molecular classifications [1–4]. HCCs with stem cell features constitute a subclass of therapeutically challenging cancers [5]. Hepatic cancer stem cells (CSCs) form a heterogeneous cell compartment as they could result from the transformation of stem/progenitor cells, but also and probably more often, from the acquisition of stem properties by liver cancer cells [5, 6]. Indeed, any hepatic cell lineage can retrodifferentiate into CSC as a result of oncogenic transformation [5] and/or inflammatory signals [7]. Such plasticity potential contributes to both intra- and inter-tumor heterogeneity of HCCs [5, 8] and makes it difficult to eradicate the whole tumor with single-agent therapies that do not address the diversity of cancer cell populations, including quiescent or slow-proliferating CSCs [9].

Recently, it has become clear that cell retrodifferentiation and subsequent phenotypic conversion were linked to metabolic shifts [10, 11]. Consistent with these observations, recent classifications have integrated cell metabolism as a discriminant parameter among HCCs [12, 13]. HCCs with liver periportal-type (HNF4α-driven) or perivenous-type (β-catenin-driven and fatty acid addicted) metabolic features belong to the non-proliferative, well-differentiated HCC class [13, 14]. Interestingly, Yang's subclasses with low and intermediate metabolic activities (gluconeogenesis, amino acid, lipid and drug metabolism) have the worst prognosis and match the poorly differentiated Hoshida's S1 and Désert's ECM and STEM subclasses [3, 12, 13]. Therefore, identifying and targeting cancer cell-specific metabolism is a promising strategy to improve HCC therapy. Several works have focused on the metabolic characteristics of tumor cells and CSCs, but few have addressed metabolic reprogramming associated with cancer cell retrodifferentiation.

[1]Inserm, Univ Rennes, INRAE, NuMeCan Institute, (Nutrition, metabolisms and cancer), Rennes, France. [2]Division of Trauma and Orthopaedic Surgery, University of Cambridge, Addenbrooke's Hospital, Hills road, Cambridge, UK. [3]Univ Rennes, CNRS, Inserm, MRIC-TEM platform, Rennes, France. [4]CHU Rennes, Pontchaillou site, Rennes, France. [5]These authors contributed equally: Florian Cabillic, Anne Corlu. ✉email: florian.cabillic@univ-rennes.fr; anne.corlu@inserm.fr

Edited by Cristina Munoz-Pinedo

Received: 9 December 2024 Revised: 16 May 2025 Accepted: 16 June 2025
Published online: 17 November 2025

We previously modelled HCC retrodifferentiation steps in two human HCC cell lines that, under defined culture conditions, display the CSC-, bipotent progenitor- and mature hepatocyte-like phenotypes [7, 15]. We reported that retrodifferentiation of human tumour-derived hepatocytes into CSCs leads to an upregulated expression of pyruvate dehydrogenase kinase 4 (PDK4), which prevents pyruvate from feeding the tricarboxylic acid (TCA) cycle. This upregulation is associated with stemness features in human HCCs [11]. Moreover, the PDK4 inhibitor dichloroacetate (DCA) improves the efficacy of chemotherapies against hepatic CSCs [11]. Unexpectedly, our transcriptomic analyses revealed that hepatic CSCs derived from tumor-derived differentiated hepatocytes ? have an increased expression of peroxisome proliferator-activated receptor (PPAR)γ, a key metabolic transcriptional modulator.

PPARγ is a master regulator of adipocyte differentiation through the control of lipid uptake, synthesis and storage, as well as glucose uptake. It also regulates a broad range of cellular functions e.g., inflammatory response, metabolism and apoptosis in various cell types [16]. Interestingly, it is a positive transcriptional regulator of PDK4 in adipocytes [17] and lung cancer cells [18]. In the liver, the predominant isoform is PPARα, which plays a crucial role in the maintenance of energy balance [19, 20]. During stress or starvation, PPARα activation spares pyruvate for gluconeogenesis *via* increased levels of PDK4, while it stimulates fatty acid oxidation (FAO) to fulfil energy needs [20, 21]. Although uncommon in the liver, PPARγ mediates anti-inflammatory and anti-fibrotic functions and maintains lipid/glucose homeostasis and insulin sensitivity in pathological conditions [22]. Regarding HCCs, PPARα is proposed as a positive prognosis marker [23]. By contrast, the role of PPARγ is controversial. Indeed, although PPARγ was mainly found to inhibit cell proliferation and HCC metastases in vitro and in mice [24–27], recent studies reported pro-tumorigenic effects in HCCs [28–30]. Likewise, in other cancers, many studies suggest anti-tumor effects of PPARγ, but pro-tumor effects are also reported [31]. Focusing on CSCs, PPARγ activation promotes the eradication of CSCs in leukemia, prostate and colorectal cancers by modulating CSC self-renewal and differentiation [32–34]. Conversely, it maintains ERBB2-positive breast CSCs [35], and PPARγ agonists increase the incidence of colorectal, renal and bladder cancers [36, 37]. It is, therefore, crucial to clarify the role of PPARs according to cell types and/or cell differentiation stages in HCCs before considering targeted therapy.

In this context, we sought to characterize the metabolic reprogramming that takes place during the differentiation/retrodifferentiation of tumour-derived hepatocytes and specify the role of PPARγ in the metabolic adaptation of hepatic CSCs. We used the human HepaRG and HBG-BC2 HCC cell lines, both characterized by high plasticity potential [15, 38]. For instance, while expression profiles of differentiated-HepaRG cells match with the periportal-type HCC subclass, which discriminates well-differentiated and favorable outcome tumors, gene expression profiles of HepaRG-CSCs are enriched in signatures related to CSCs, metastasis, recurrence and match with Désert's STEM and Hoshida's S1 HCC signatures, both associated with poor prognosis [3, 13]. Here, we show that these hepatic CSCs, whose transcriptome matches the early stages of mouse development, have reduced mitochondrial biogenesis and cell respiration. In parallel, they adopt a glycolytic profile and store lipids into droplets until they leave their slow-proliferating state and commit to a differentiation program. Our results highlight, for the first time, a balanced expression of PPARα and PPARγ along the tumor-derived hepatocyte differentiation/retrodifferentiation process. They reveal a role of PPARγ in the metabolic rewiring of hepatic CSCs, which contributes to chemoresistance. We show that PPARγ has not only anti-proliferative but also pro-stemness properties. Our results show that PPARγ, whose expression is increased in the human HCC STEM subclass, is a negative prognostic factor in three human HCC cohorts. At last, we demonstrate that PPARγ inhibition synergizes with cisplatin or sorafenib, notably by limiting PDK4 expression and reactivating the mitochondrial production of reactive oxygen species (ROS).

MATERIALS AND METHODS

Patient samples and cohorts

Five publicly available HCC transcriptomic datasets were used: Data for the Roessler's patient cohort (238 HCCs) are accessible through GEO Series accession number GSE14520; the Cancer Genome Atlas Liver Hepatocellular Carcinoma cohort (TCGA-LIHC; 370 HCCs) through the link https://www.cancer.gov/tcga, the International Cancer Genome Consortium cohort (ICGC; 232 HCCs) project LIRI-JP through the link https://dcc.icgc.org/projects/LIRI-JP, the data for the Kaposi-Novac's (GSE12443) and Wurmbach's (GSE6764) patient cohorts.

Mouse liver development

Two datasets of mouse liver development time-course were used: GSE90047 ($n = 21$) [39] and GSE13149 ($n = 25$) [40].

Cell lines

We used 2 human HCC cell lines established in our laboratory, HBG-BC2 [15] (Inserm UMR 1317, ex Inserm U 49) and HepaRG [41] (Inserm UMR 1317, ex Inserm UMR 552, Patent number US7456018). We also used 2 commercial HCC cell lines, HepG2 (ECACC Cat# 85011430, RRID:CVCL_0027), Huh7 (ECACC Cat# 01042712, RRID:CVCL_2957) and Huh6 cells (RRID:CVCL_4381), a kind gift of Dr. Christine Perret, Institut Cochin [42]. HepaRG cells were cultured as previously described [41]. Briefly, cells were seeded at 2.7×10^4 cells/cm^2 in William's E medium (Gibco, 22511-022) supplemented with 10% fetal bovine serum (FBS), 100 U/ml penicillin (Gibco, 15070-063), 100 µg/ml streptomycin (Gibco, 15070-063), 5 µg/ml insulin (Sigma-Aldrich, I5500), 5×10^{-5} M hydrocortisone hemisuccinate (Upjohn, Serb) and 2 mM glutamine (Gibco, 25030-024). Progenitors (D4) are cells obtained 4 days after seeding; committed/confluent cells (D15) correspond to cells 2 weeks after seeding. After this stage, the medium was supplemented with 2% DMSO (Sigma-Aldrich, D4540) and the cells were cultured for a further 2 weeks to enhance differentiation (differentiated cells, D30) (Fig. S1A). HBG-BC2 cell line was cultured in HepaRG medium without DMSO and maintained 2 weeks at confluency to reach differentiation. HepG2, Huh6 and Huh7 were cultured in DMEM medium (Sigma-Aldrich, M2279) supplemented with 10% FBS, 2 mM glutamine, 100 U/ml penicillin and 100 µg/ml streptomycin. HCC cell spheres and HepaRG-side population were obtained as previously described [11]. For spheres, progenitor HepaRG or proliferating HCC cells were cultured in ultra-low attachment plates and stem cell medium consisting of DMEM/F12 medium (Gibco, 11330-032) supplemented with 20% knockout serum replacement (Gibco, 10828-028), 1 mM L-glutamine, 1% nonessential amino acids (Gibco, 11140050), 0.1 mM β-mercaptoethanol (Gibco, 31350010) and 4 ng/ml fibroblast growth factor 2 (Miltenyi Biotec, 130-093-840). HepaRG-SP was obtained from the progenitor population by sorting cells that are able to efflux Hoescht 33342 [11]. Experiments on HepaRG-SP cells were performed within 24 hours after seeding in HepaRG medium without DMSO to limit cell proliferation and differentiation. Note that some experiments were performed only with HepaRG-spheres, but not with HepaRG-SP, because of the small amount of SP available.

Oxygen consumption and glycolysis measurements

Respiration and glycolysis were measured by Seahorse XFe Analyzer (Agilent). Respiration was assessed by successive injections of oligomycin (2 µM), carbonyl cyanide-4 (trifluoromethoxy) phenylhydrazone (FCCP, 1 µM) and the combination of antimycin A/rotenone (1 µM) into the culture medium (Seahorse XF Cell Mito Stress Test Kit, Agilent Technologies, 103015-100). Glutaminolysis was performed by using a respiration kit (Seahorse XF Cell Mito Stress Test Kit, Agilent Technologies, 103015-100). 24 h before the Seahorse measurements, cells were placed in a glutamine-deprived medium or were treated with 1 mM of a glutamine antagonist called 6-Diazo-5-oxo-L-norleucine (DON). Glycolysis was assessed by injection of glucose (10 mM), oligomycin (1 µM) and 2-deoxy-D-glucose (2-DG) (50 mM) (Seahorse Glycolysis Stress Test Kit, Agilent Technologies,

103020-100). Analyses were performed with Wave software 2.3.0. Results were normalized to cell number obtained by fluorescence intensity of Hoechst 33342 correlated with nucleus count performed at 460 nm on a POLARstar Omega plate reader (BMG Labtech).

Assessment of FAO with [U-^{14}C]palmitic acid

FAO was assessed by measuring the acid-soluble radiolabeled metabolites resulting from the mitochondrial oxidation of [U-^{14}C]palmitic acid as previously described [43]. Cells were washed with warm PBS (Gibco, 10010023) and incubated in phenol red-free William's E medium (Gibco, A1217601) containing 1% fatty acid-free BSA (Sigma-Aldrich, A8806), [U-^{14}C]palmitic acid (Perkin Elmer, NEC534050UC), 100 µM cold palmitic acid (Sigma-Aldrich, P5585), 1 mM L-carnitine (Sigma-Aldrich, C0283). After 3 hours of incubation, perchloric acid, final concentration 6%, (Fisher Scientific, 12993564) was added, and plates were centrifuged at 2000 × *g* for 10 min. The supernatant was counted for [^{14}C]-labelled acid-soluble β-oxidation products using a Tri-Carb 4910TR liquid scintillation counter (Perkin Elmer). Results were normalized to cell number as described for oxygen consumption.

Assessment of de novo lipogenesis from [2-^{14}C]acetic acid

De novo lipogenesis was assessed by measuring newly synthesized radiolabeled lipids from [2-^{14}C]acetic acid, using a protocol from Byrne et al. [43, 44]. Cells were washed with warm PBS and incubated for 3 hours with phenol red-free William's E medium containing 1% fatty acid-free BSA, [2-^{14}C] acetic acid (Perkin Elmer, NEC553050UC) and 50 µM cold acetic acid (Sigma-Aldrich, S5636). Cells were then washed with PBS before adding a mix of hexane/isopropanol (3 V/2 V) (Sigma-Aldrich, 139386 and I9516) and incubated for 1 hour at room temperature for lipid extraction. After transfer in microtubes, hexane and PBS were added to have a hexane/isopropanol/PBS ratio of 6 V/2 V/3 V. Microtubes were centrifuged at 1000 × *g* for 5 min, and radiolabeled lipids were counted in the upper phase with a Tri-Carb 4910TR liquid scintillation counter (Perkin Elmer). Results were normalized to cell number as described for oxygen consumption.

Statistical analysis

Microarray data (GSE75752 and GSE112123) were provided by experiments previously performed in the laboratory [11]. mRNAs were obtained from biological replicates ($n = 4$) of HepaRG-SP, HepaRG-spheres, and HepaRG cells recovered 4 (HepaRG-progenitor), 15 (HepaRG-committed/confluent) and 30 (HepaRG-differentiated) days of culture (Fig. S1A). To determine genes significantly deregulated between progenitors (day 4 after seeding) and differentiated cells (day 30 after seeding), a t-test was performed with the package R Limma. To determine genes significantly deregulated between HepaRG-CSC (spheres and SP) and differentiating (progenitor, committed/confluent and differentiated) cells, a one-way ANOVA was performed. Numerical data comparisons were analyzed using GraphPad Prism software (Version 7.0, GraphPad, San Diego, CA). Significance was assessed by parametric (Student *t* test, one-way ANOVA or two-way ANOVA) and nonparametric (Mann–Whitney test or Kruskal–Wallis test) methods according to the results of the normality test. Results are expressed as mean ± SEM.

RESULTS

Retrodifferentiation of HepaRG cells alters both the expression of mitochondria-related genes and the mitochondrial network

The acquisition of fetal/hepatoblast characteristics is a well-known feature of hepatic carcinogenesis and is associated with the severity of HCCs [4]. Retrodifferentiation, which occurs during liver carcinogenesis and HCC progression, mirrors fetal development. We previously showed that the transcriptomic data of HepaRG-side population (SP) and HepaRG-sphere-forming cells (Spheres) match those of both the STEM [12, 13]/S1 [3] HCC subclasses and human embryonic stem cells [11]. Here, we sought to clarify to what extent HepaRG differentiation stages (from Spheres, SP, bipotent progenitors, through committed/confluent cells and to differentiated cells, represent different stages of hepatic organogenesis (Fig. S1A). To this end, we integrated HepaRG transcriptomic data with two time-course experiments of mouse liver development (GSE90047 [39]) and (GSE13149 [40]). Hierarchical clustering of transcriptomes from embryonic stages E10.5 through E18.5 and from E11.5 through post-natal days 0 (birth) –21 (weaning) to adult liver, based on the progenitor vs differentiated HepaRG signatures (DEG, $P \leq 0.05$, FC > 2, Table S1) reveals two clusters (Fig. 1A). Spheres, SP and progenitor cells clustered with early embryonic livers (E10.5 or E11.5 to 14.5) and committed/confluent and differentiated cells clustered with post-natal mouse liver samples (post-natal day 7 to adult liver). These findings indicate that the selected differentiation stages of HepaRG cells correspond to the developmental stages of mouse liver, from the emergence of the liver bud to the adult liver and conversely. Therefore, HepaRG cell plasticity may correctly reflect the differentiation/retrodifferentiation processes and the phenotypic diversity of HCCs.

Then, we characterized the metabolic reprogramming of HepaRG-CSCs modelled by HepaRG-spheres and HepaRG-SP [7, 11]. We identified 6115 differentially expressed genes (DEG, $p \leq 0.05$, FC > 1.5) between the HepaRG-CSCs and the HepaRG differentiating cells i.e., progenitors, committed/confluent and differentiated cells (Table S2). Unsupervised gene set enrichment analysis (GSEA) reveals that the transcriptomic program of HepaRG-CSCs was negatively correlated with oxidative phosphorylation (OXPHOS), TCA cycle and pyruvate metabolism (Fig. S1B). Accordingly, supervised GSEA shows a negative correlation of HepaRG-CSCs with the Mitocarta gene list [45], a compendium of 1136 human genes encoding mitochondria proteins and pathways (Fig. 1B). Among these genes, 471 mitochondria-related genes, accounting for 7.7% of the DEG, are modulated (Fig. 1D, Table S3). Specifically, 160 Mitocarta genes are upregulated in HepaRG-CSCs while 311 genes, involved in the top three pathways (TCA cycle, mitochondrial respiratory chain and ATP synthesis), are downregulated (Fig. 1C, D). Next, we integrated the 471 Mitocarta DEG with the 550-gene classifier signature that defines the four HCC subclasses (perivenous, periportal, extracellular matrix, stem) in Désert's classification [13]. We show that the genes downregulated in HepaRG-CSCs are also downregulated in the STEM subclass with respect to the periportal and perivenous subclasses (Fig. 1E). This prompted us to study the consequences of transcriptional changes on mitochondria number and network organization. Electron microscopy confirms a reduced number of mitochondria in HepaRG-CSCs compared with differentiated cells (Fig. 1F). This result is supported by both the quantification of mitochondrial DNA content and mitochondrial mass (Fig. 1G). Accordingly, the expression of PPARγ coactivator 1-alpha *(PPARGC1A/PGC1A)*, a master regulator of mitochondrial biogenesis, is low in HepaRG-CSCs and gradually increases across the proliferation and epithelial commitment phases of HepaRG-progenitors (Fig. 1G). In addition, confocal microscopy analyses revealed that HepaRG-CSCs harbor a mitochondrial network with significantly fewer branching points (Fig. 2A).

HepaRG-CSCs rewire their metabolism and slow down their proliferation rate

A high-branched mitochondrial network is thought to increase OXPHOS efficiency and energy supply [46]. This prompted us to study the metabolism of HepaRG cells during the differentiation/retrodifferentiation process. HepaRG-CSCs adopt a glycolytic profile with both high glycolysis level (Fig. 2B) and increased lactate production (Fig. 2C). Conversely, lower mitochondrial respiration rate is observed in immature than in differentiated HepaRG cells (Fig. 2B). Moreover, FAO (Fig. 2C) and glutaminolysis (Fig. S1C) are low in HepaRG-CSCs. In keeping with the reduced FAO, low β-hydroxybutyrate levels (Fig. 2C) suggest a decrease in ketogenesis. In addition, an accumulation of neutral lipids is observed in HepaRG-spheres (Fig. 2C) and -SP [4]. This accumulation probably results from increased fatty acids (FAs) uptake through increased expression of the FA transporter FAT/CD36

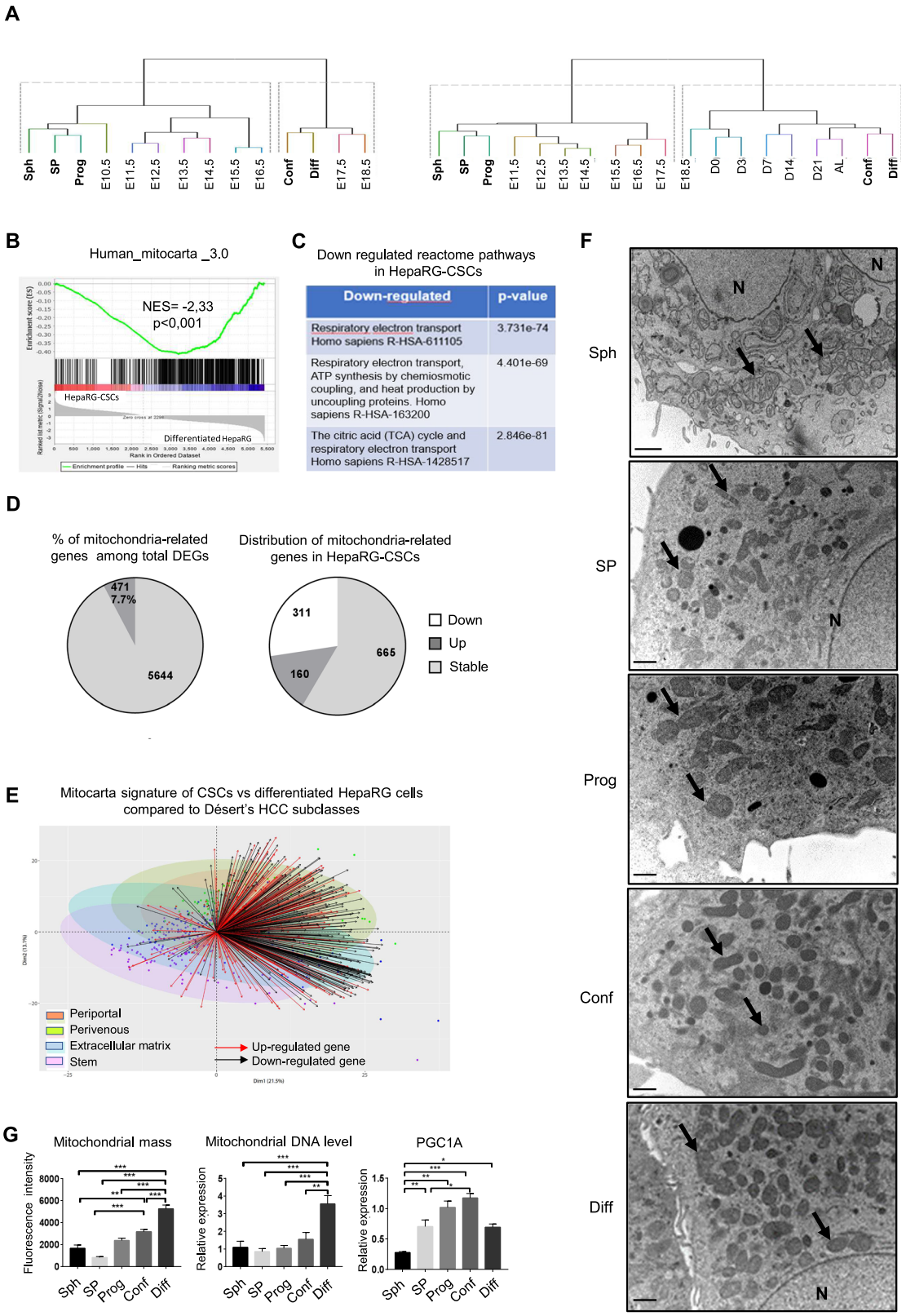

rather than from de novo lipogenesis, which is very low in HepaRG-CSCs (Fig. 2C). It should be noted that HepaRG-spheres and -SP, although both immature cells display some differential metabolic features. Notably, mitochondrial respiration and FAO are higher in HepaRG-SP. These differences are likely related to the resting state or cell cycle rate of the cells. Indeed, HepaRG-spheres express high levels of early G1 and G1 phase markers (*JUN, CDKN1A, CDK4 and CCND1*) but not the S and M phase markers (*CDK1* and *CCNB1*), showing that they are stalled in G1 (Fig. S1D). HepaRG-SP expresses high levels of early G1 and G1 phase

Fig. 1 Downregulation of mitochondria-related gene expression in HepaRG-CSCs. A Integration of differentially expressed HepaRG genes (DEG, $P \leq 0.05$, FC > 2) between progenitors (Prog, day 4 after seeding) and differentiated cells (Diff, day 30 after seeding) with orthologs from two mouse liver development mRNA datasets: Left panel: GSE90047 [39], from embryonic stages E10.5 through E18.5; Right panel: GSE13149 [40], from E11.5 through post-natal days 0 (birth)—21 (weaning) to adult liver. HepaRG cells: Sph = Spheres; SP = side population; Conf=committed/confluent cells at day 15 after seeding; Diff = differentiated cells at day 30 after seeding. Mouse liver development: *E*, days post-coitum (detection of the vaginal plug); *D*, post-natal days. Manhattan and Ward. D2 were respectively used as distance and clustering methods. **B** GSEA plot for mitochondria-related genes referenced in Mitocarta 3.0; NES, normalized enrichment score. **C** Reactome pathways related to DEG in HepaRG-CSCs. **D** Left pie chart: percentage of mitochondria-related genes among total differentially expressed genes (DEG) between immature and differentiating HepaRG groups; Right pie chart: Mitocarta genes upregulated (dark grey) or downregulated (white) in HepaRG-CSCs. **E** Biplot showing the distribution of the 471 DEG belonging to Mitocarta among Désert's HCC subclasses: PP periportal, PV perivenous, ECM extracellular matrix. **F** Electron microscopy of HepaRG cells: Sph = spheres, SP = side population, Prog = progenitors, Conf = committed/confluent, Diff=differentiated. Black arrows point out mitochondria; N, nucleus. **G** Mitochondrial DNA assessed by RT-qPCR ($n \geq 4$). Mitochondrial mass evaluated by flow cytometry using Mitotracker Green® ($n \geq 6$). *PPARGC1A/PGC1A* mRNA expression relative to HepaRG-progenitors ($n \geq 3$). *$p < 0.05$, **$p < 0.01$, ***$p < 0.001$.

markers (*JUN, FOS, CDK4, CDKN1B*) but also intermediate levels of *CDK1* and *CCNB1*, disclosing a slow-cycling phenotype. As expected, progenitors are active proliferating cells, expressing high levels of S and M phase markers, whereas committed/confluent and differentiated HepaRG cells barely express these markers (Fig. S1D).

HCC cell lines adopt distinct metabolic features according to their plasticity potential and proliferation rates

We completed our study by exploring the metabolism of other HCC cell lines (Fig. S2A). Like HepaRG, HBG-BC2 (BC2) shows strong potential for plasticity and differentiation, as evidenced by the inverse expression profile of stemness (*CD44*) and differentiation (*aldolase B*) markers in spheres and 15-day-old committed/confluent cells (Fig. 3A). Noteworthy, both HepaRG- and BC2-CSCs form small spheres (Fig. S2A). They have a low *PGC1α* expression (Fig. S2B) and adopt a similar metabolism i.e., a glycolytic profile with high lactate production, low mitochondrial respiration and de novo lipogenesis, lipid droplet accumulation and higher *FAT/CD36* expression than their differentiated counterparts (Fig. 3B, C). Of note, FAO and β-hydroxybutyrate levels are very low even in differentiated BC2 cells compared to differentiated HepaRG cells (Fig. 3C). Consistent with the high expression of *FAT/CD36* and lipid accumulation, lipid analysis shows higher amounts of free FAs, triglycerides and cholesterol esters in HepaRG- and BC2-spheres (Fig. 3D). In addition, HepaRG- and BC2-spheres are characterized by higher saturated/unsaturated FA ratio and phospholipid content compared with differentiated cells (Fig. 3D). In contrast to HepaRG and BC2, three other cell lines, Huh6, Huh7 and HepG2, have reduced plasticity and formed spheres that contained proliferative rather than immature cells (Figs. 3A and S2A). Mitochondrial respiration is high in spheres derived from Huh6, Huh7 and HepG2 cell lines, whereas adherent cells mainly rely on glycolysis (Fig. 3B). In addition, only slight changes in FAO, *FAT/CD36* expression and neutral lipid accumulation are apparent when comparing spheres and adherent proliferative Huh6, Huh7 and HepG2 cells (Fig. 3C).

High *PPARG*/*PPARA* ratio is associated with poor prognosis in human HCC

Changes in lipid metabolism and up-regulated transcription of *PPARG* [11] in HepaRG-CSCs prompted us to further investigate the role of PPAR family members, known as key regulators of cell metabolism. Unlike *PPARA*, *PPARG* expression is high in HepaRG- and BC2-CSCs, with *PPARG1* predominating over *PPARG2* (Fig. 4A and Fig. S2C). *PPARG* expression likely results from the activation of the PIK3/AKT signaling pathway as Ly294002, which inhibits the AKT upstream activator PI3K, reduces both AKT phosphorylation and *PPARG* expression in HepaRG-progenitors (Fig. 4A). Throughout the differentiation process, *PPARG* expression decreases whereas *PPARA* expression increases, and *PPARD* is fairly stable (Fig. 4A).

From 2 transcriptomics datasets representing stepwise carcinogenic process (cirrhosis, dysplasia and HCC), we observed that *PPARG* expression is unchanged between pre-neoplasic lesions and early HCC (Fig. S2D) [47, 48]. In contrast, its expression was higher in advanced HCC versus cirrhotic tissue (Fig. S2D) [47]. In parallel, *PPARA* expression was downregulated. Interestingly, Kaplan-Meier survival analyses on TCGA-LIHC [49] (Fig. 4B), ICGC and Roessler's [50] (Fig. S3A, B) HCC patient datasets reveal that high *PPARG* expression is related to worse overall survival. By contrast, expression of *PPARA* is associated with better prognosis in TCGA-LIHC (Fig. 4B) and ICGC cohorts (Fig. S3A). Moreover, *PPARG* and *PPARA* are positively and negatively correlated, respectively, with alpha-fetoprotein (AFP), a marker of aggressiveness in HCC, both in TCGA-LIHC and Roessler's datasets (Figs. 4C and S3C). In addition, high *PPARG* expression matches the poor outcome Désert's STEM HCC subclass, whereas high *PPARA* expression is found in perivenous-type and periportal-type subclasses, which have better prognosis (Fig. 4D). Fifty-eight HCC tumor tissues were analyzed by immunohistochemistry (IHC), nine of which were positive for PPARγ. Importantly, IHC revealed nuclear localization of PPARγ in the tumor and in tumor nodules invading adjacent stromal tissues (Fig. 4E). Clinical and biological data and risk factors for HCC occurrence are given in Table S4.

PPARγ favors stemness and metabolism rewiring in hepatic tumor cells

To get more insight into the role of PPARγ in HCC metabolism, we carried out silencing experiments or agonist treatments using HepaRG- and BC2-spheres, which highly express PPARγ. As expected, the mRNA levels of *PPARG* are reduced in the presence of siPPARG whereas PPARγ-agonist rosiglitazone does not affect its expression (Figs. 4A, 5A and S4A). Inhibiting PPARγ expression by siRNA transfection drastically reduces the sphere number and causes significant cell death, whereas treatment with the PPARγ agonist rosiglitazone induces no change in cell viability (Fig. 5A). Due to the cell number requirement, we next used proliferative HepaRG-progenitors and BC2 cells that also express PPARγ at significant levels (Figs. 5B–E, 6A–C). Treatment with rosiglitazone slows down cell proliferation, thus leading to empty areas in culture plates and reduces ATP levels unrelated to apoptosis induction (Fig. 5B). Treatment also increases the expression of known PPARγ target genes such as *PDK4*, *FAT/CD36* and perilipin2 (*PLIN2*), which contributes to the formation and stability of lipid droplets (Fig. 5C). Interestingly, rosiglitazone treatment results in decreased expression of the epithelial marker E-cadherin (*CDH1*) associated with increased expression of the transcription factor *SNAIL* and the stem cell marker *KLF4*, showing that cells commit to EMT and stemness (Fig. 5C). Consistent with rosiglitazone-induced retrodifferentiation, cells have a less extensive and branched mitochondrial network (Figs. 5D and S5B) as well as lower mitochondrial respiration (Fig. 5E). In accordance, attenuation of PPARγ expression (RNA and protein levels) by siRNA

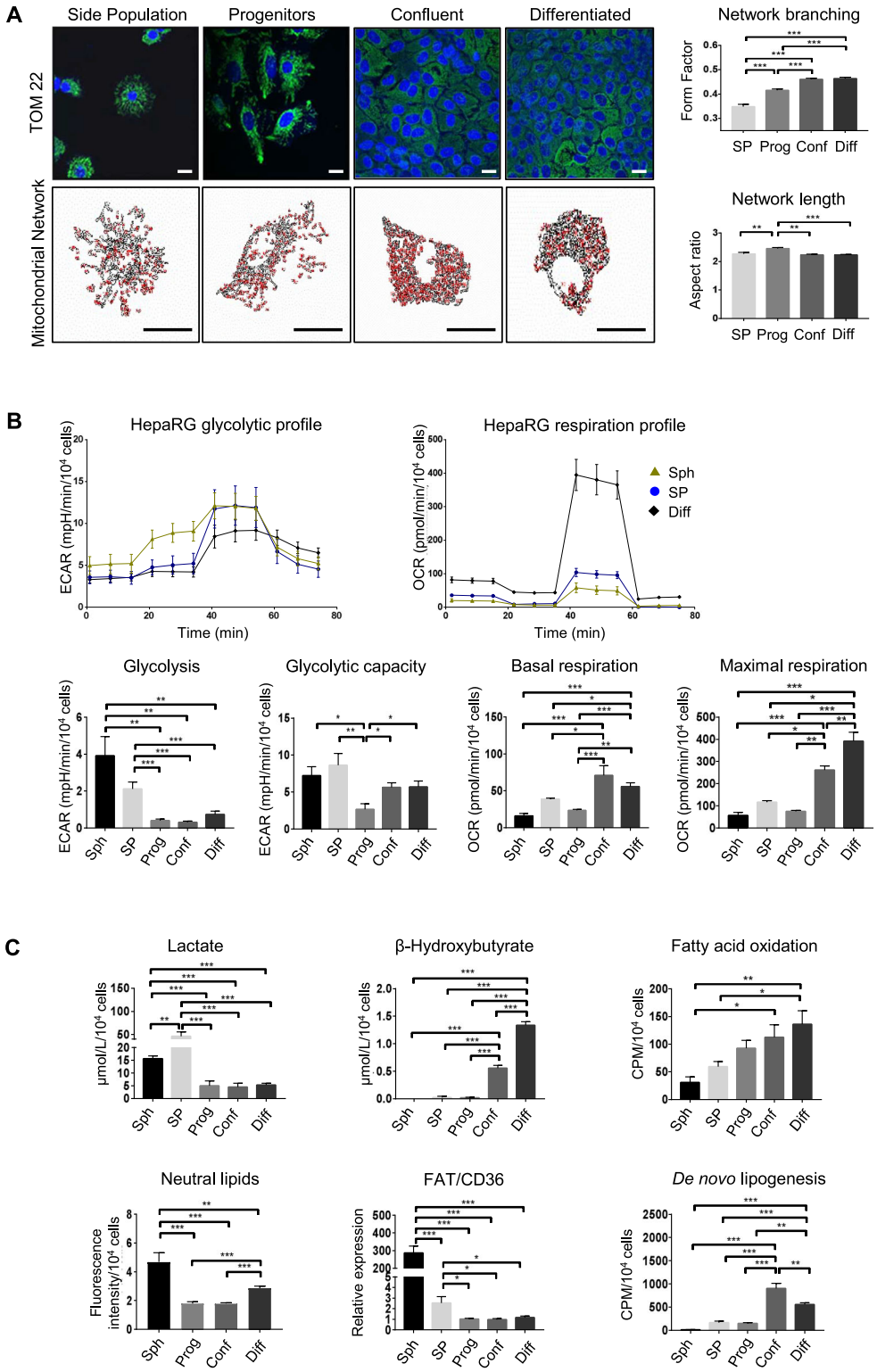

Fig. 2 Metabolic reprogramming during differentiation/retrodifferentiation process in HepaRG cells. A Confocal microscopy of the mitochondrial protein TOM22 immunostaining in HepaRG cells: SP = side population, Prog = progenitor, Conf = committed/confluent, Diff = differentiated; Bar = 20 µm. Mitochondrial network length and branching analyzed using ImageJ ($n = 3$); Bars = 20 µm. **B** Representative glycolytic (extracellular acidification rate, ECAR) and mitochondrial respiration (oxygen consumption rate, OCR) profiles obtained with Seahorse analyzer: Sph = HepaRG-spheres. Glycolysis, glycolytic capacity, basal and maximal respiration ($n \geq 5$). **C** Lactate and β-hydroxybutyrate in culture supernatant assessed by absorption spectrophotometry ($n \geq 3$). FAO and de novo lipogenesis were assessed by quantifying the radioactivity subsequent to ^{14}C-palmitate and ^{14}C-acetate incorporation, respectively ($n \geq 4$). FAT/CD36 mRNA expression relative to HepaRG-progenitors ($n = 4$). Neutral lipid content assessed by Nile red staining ($n \geq 5$). *$p < 0.05$, **$p < 0.01$, ***$p < 0.001$.

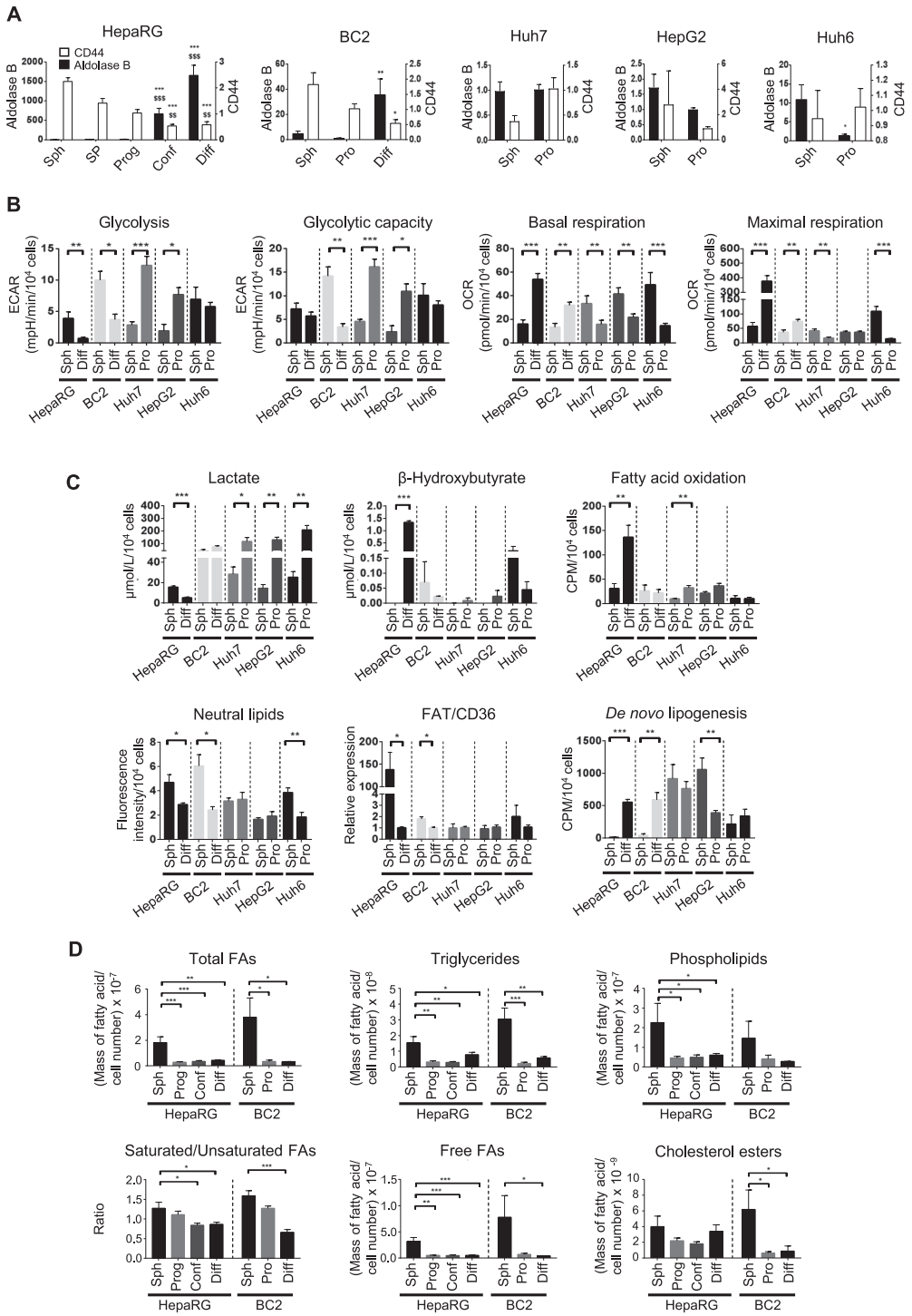

Fig. 3 Metabolism rewiring in HCC cell lines. A *Aldolase B* (left *y* axis) and *CD44* (right *y* axis) mRNA expression throughout the culture of HepaRG, BC2, Huh7, HepG2 and Huh6 cell lines: Sph = spheres, SP = side population, Prog = progenitors, Conf = committed/confluent, Diff = differentiated and Pro = proliferative. Results are expressed relative to progenitors for HepaRG or proliferative cells for BC2, Huh7, HepG2, and Huh6 ($n \geq 3$). Comparison with spheres *$p < 0.05$, **$p < 0.01$, ***$p < 0.001$; comparison with SP \$ $p < 0.05$, \$\$ $p < 0.01$, \$\$\$ $p < 0.001$. **B** Glycolysis, glycolytic capacity, and basal and maximal respiration were assessed with the Seahorse analyzer for HepaRG, BC2, Huh7, HepG2, and Huh6 ($n \geq 3$). **C** Lactate and β-hydroxybutyrate were assessed in culture supernatants by absorption spectrophotometry ($n \geq 3$). FAO and de novo lipogenesis were assessed by quantifying the radioactivity subsequent to ^{14}C-palmitate and ^{14}C-acetate incorporation, respectively ($n \geq 3$). *FAT/CD36* mRNA expression is relative to progenitors for HepaRG and proliferative cells for BC2, Huh7, HepG2 and Huh6 ($n \geq 3$). Neutral lipid content assessed by Nile red staining ($n \geq 3$). **D** Quantification by gas chromatography-mass spectrometry of fatty acids (FAs) from cell total lipids (total FAs), triglycerides, phospholipids, cholesterol esters and free FAs in HepaRG and BC2 at different stages of differentiation. The saturated/unsaturated FA ratio is calculated from data obtained with the total lipid pool. Results are normalized by the number of cells ($n \geq 3$). *$p < 0.05$, **$p < 0.01$, ***$p < 0.001$.

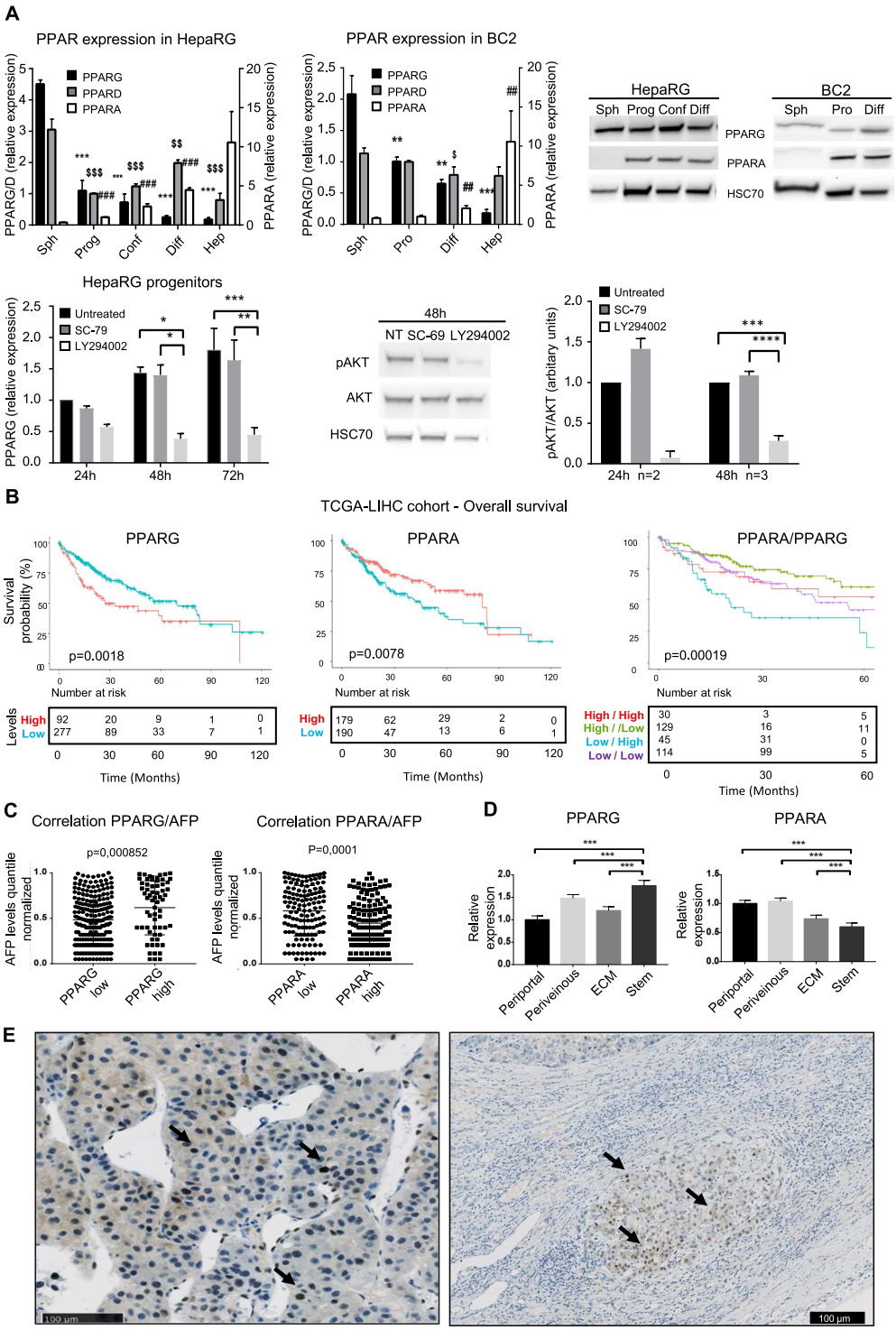

Fig. 4 High *PPARG* expression is associated with stem phenotype and poor prognosis in human HCC. A Upper left panel: *PPAR* mRNA expression throughout the differentiation process of HepaRG and BC2 cells: Sph=spheres, SP=side population, Prog = progenitors, Conf = committed/confluent, Diff = differentiated, Pro = proliferative, Hep = freshly isolated human hepatocytes. Results are expressed relative to HepaRG-progenitors or BC2-proliferative cells ($n \geq 3$). *, $ and # for *PPARG*, *PPARD* and *PPARA*, respectively; $ $p < 0.05$; **, $$, ##$p < 0.01$; ***, $$$, ###$p < 0.001$; all compared with spheres. Upper right panel: western blot of PPARγ, PPARα, and HSC70 in HepaRG and BC2 cells. Lower left panel: *PPARG* mRNA expression in HepaRG-progenitors treated with SC-79 or LY294002 during 24, 48, or 72 h. Lower right panel: western blot and densitometry of AKT and phosphoAKT (pAKT) in HepaRG progenitors treated with SC-79 or LY294002 during 24 or 48 h. *$p < 0.05$; **$p < 0.01$; ***$p < 0.001$. **B** Overall survival according to *PPARG* and/or *PPARA* expression in the TCGA-LIHC cohort. **C** Correlation between *PPARG* and *PPARA* expression and AFP level in the TCGA-LIHC cohort. **D** *PPARG* and *PPARA* expression in the Désert's HCC subclasses. Results are expressed relative to *PPARG* and *PPARA* levels in the periportal subclass. ***$p < 0.001$. **E** Immunostaining of PPARγ in human HCC. Both the tumor (left) and a tumor nodule invading adjacent tissue (right) show nuclear and cytoplasmic signal. Black arrows indicate a nuclear localization of PPARγ.

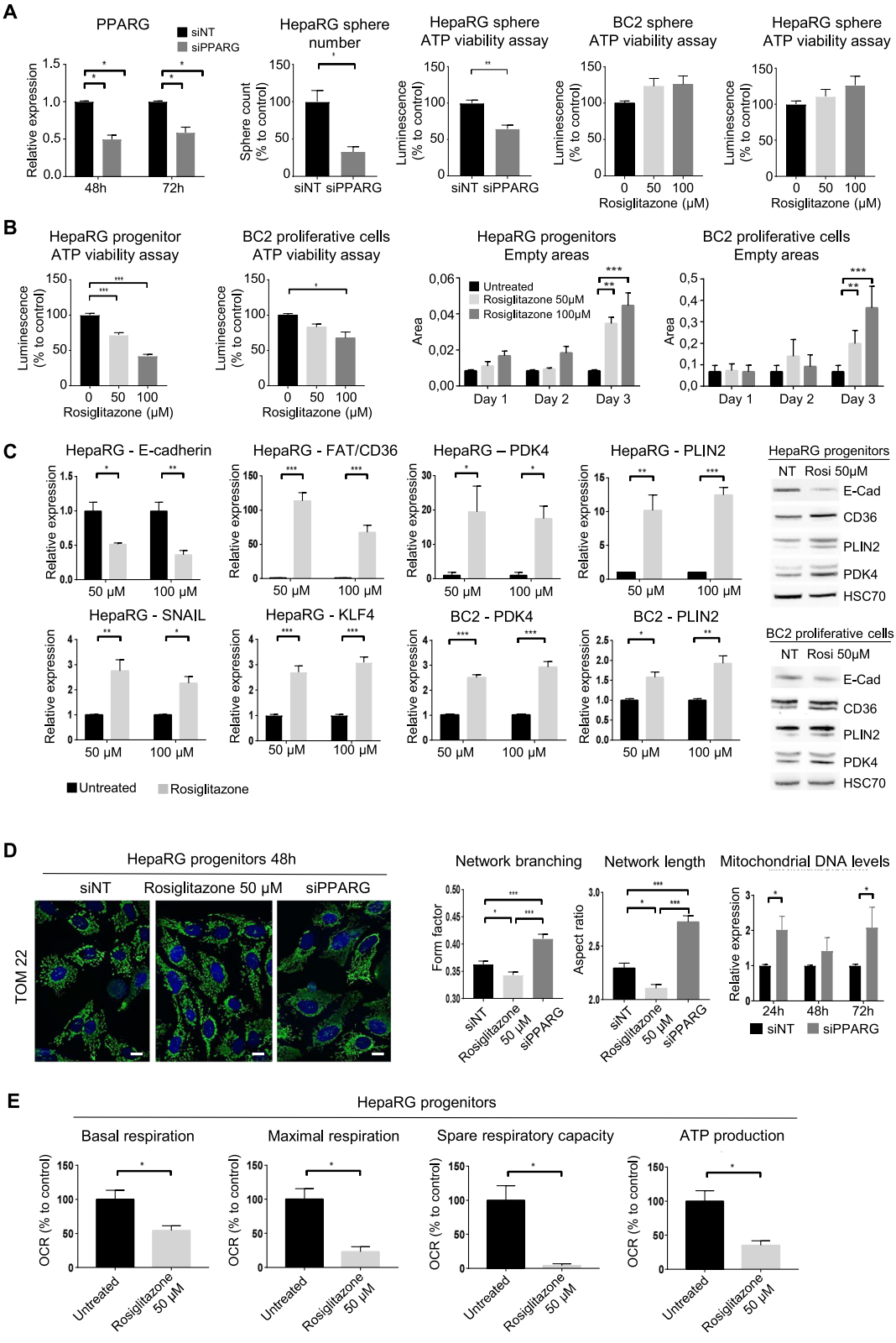

(Figs. 6B and S4B) induces a decreased expression of *PDK4* and *PLIN2* (Fig. 6B). This decrease is associated with increased respiratory capacities and proton leak reflecting suboptimal efficacy of the respiratory chain (Fig. 6C). In addition, *PPARG*-invalidated cells contain an increased level of mitochondrial DNA and exhibit an extensive and high-branched mitochondrial network at 48 h (Fig. 5D) and 72 h (Fig. S5B). Overall, *PPARG* invalidation leads to decreased cell viability (Figs. 6A, 7C).

PPAR targeting improves efficacy of HCC therapies in vitro

We have previously shown that HepaRG-progenitors resistant to sorafenib or cisplatin express increased mRNA levels of *PDK4* and

Fig. 5 PPARγ activation triggers retrodifferentiation and metabolic reprogramming. A *PPARG* mRNA expression 48 h after transfection of HepaRG-spheres with siNon-targeting (siNT) and si*PPARG* ($n = 3$). Sphere number and ATP viability assay 48 h after seeding of transfected HepaRG cells in sphere culture medium ($n = 3$). ATP viability assay of HepaRG- and BC2-spheres after treatment with 50 µM or 100 µM rosiglitazone during 72 h ($n = 4$). **B** ATP viability assay of HepaRG-progenitors and BC2-proliferative cells after treatment with 50 µM or 100 µM rosiglitazone during 72 h ($n = 3$). HepaRG and BC2 proliferation assessed by quantifying empty areas using ImageJ, 3 days after seeding. ($n = 3$). **C** mRNA expression of E-cadherin (*CDH1*), fatty acid transporter *FAT/CD36*, pyruvate dehydrogenase kinase *PDK4*, perilipin2 (*PLIN2*), EMT-inducing transcription factor *SNAIL* and stem-related marker *KLF4* in HepaRG-progenitors and BC2-proliferative cells after treatment with rosiglitazone (50 or 100 µM) during 72 h ($n = 3$), and western blot of E-cadherin (E-cad), CD36, PLIN2, PDK4, and HSC70 (loading control) in HepaRG progenitors or BC2 proliferating cells treated or not (NT) during 72 h with 50 µM rosiglitazone. **D** Confocal microscopy of mitochondrial protein TOM22 immunostaining in HepaRG-progenitors 48 h after treatment with 50 µM rosiglitazone or transfection with si*PPARG*. Bar = 10 µm. Mitochondrial network branching and length analyzed using ImageJ ($n = 3$). Mitochondrial DNA assessed by RT-qPCR, 24 h, 48 h, and 72 h after transfection of HepaRG-progenitors with si*PPARG* ($n = 4$). **E** Basal respiration, maximal respiration, spare respiratory capacity and respiration linked to ATP production assessed with Seahorse analyzer in HepaRG-progenitors treated by rosiglitazone 50 µM during 48 h ($n = 3$). Results are expressed relative to untreated cells or siNT. *$p < 0.05$, **$p < 0.01$, ***$p < 0.001$.

that the combination of chemotherapy with the PDK4 inhibitor (DCA) is effective in killing immature HCC cells [11]. Here, we show that sorafenib-resistant progenitors also express higher levels of *PPARG*, a master regulator of *PDK4*, while their *PPARA* expression remains unchanged (Fig. 7A). Interestingly, targeting either PDK4 with DCA or *PPARG* with siRNA reactivates mitochondrial respiration (Fig. 6C, D) and increases ROS production (peroxide and superoxide anions) (Figs. 7B and S4C), which hepatic CSCs fail to scavenge, unlike differentiated cells (Fig. S4C). Indeed, most of the metabolic redox regulatory genes are less expressed in immature than in differentiated HepaRG cells (Fig. S5A). As a consequence, similar to DCA treatment, si*PPARG* transfection induces cell death of HepaRG-progenitors and BC2 proliferating cells, and the dual inhibition of PPARγ by siRNA transfection and PDK4 by DCA proves synergistic in reducing cell viability (Fig. 7C). In addition, *PPARG* invalidation or PPARγ antagonist T0070907 also synergizes with sorafenib or cisplatin (Fig. 7C, D). A decrease in cell viability is associated with increased ROS production and lipid peroxidation, as shown by malondialdehyde accumulation in the culture medium (Fig. 7E). To confirm the involvement of ROS in cell death mediated by PPARG inhibition, we aimed to scavenge ROS by N-acetylcysteine (NAC). As expected, NAC reduces ROS production, lipid peroxidation and cell death (Fig. 7E).

The better outcome of patients with high *PPARA* expression in the TCGA-LIHC and ICGC cohorts could result from the metabolic effects of PPARα (Figs. 4B and S3B). We hypothesized that, unlike PPARγ, PPARα activation increases mitochondrial activity without generating high levels of PDK4, which contributes to chemotherapy resistance in hepatic CSCs. Accordingly, the PPARα agonist clofibrate slightly increases mitochondrial network length in HepaRG-progenitors (Fig. S5C), slightly modulates *PPARG* expression and induces PDK4, but at much lower levels than PPARγ agonist rosiglitazone (Fig. S4A). Last, we confirmed this hypothesis using HepaRG- and BC2-spheres. Treatment with clofibrate alone does not reduce cell viability, but the combination of clofibrate with sorafenib, cisplatin or DCA reduces cell viability more than monotherapies (Fig. 7F).

DISCUSSION

Using several HCC cell lines, including HepaRG and HBG-BC2 cells that exhibit well-characterized differentiation and retrodifferentiation potential [7, 11, 15], we showed that hepatic CSCs derived from retrodifferentiation of differentiated tumor-derived hepatocytes express *PPARG* and adopt a specific metabolic profile associated with chemoresistance. Although oxidative metabolism is critical for differentiated tumor-derived hepatocytes, hepatic CSCs are characterized by low OXPHOS, mitochondrial FAO, de novo lipogenesis and high glycolytic activity. Hepatic CSCs also accumulate lipid droplets, where the triglycerides can be mobilized to fulfill energy needs. Importantly, this metabolic phenotype is reversible and not mutation-driven. Indeed, HepaRG cells are mutated in the *hTERT* promoter [51], whereas BC2 cells are mutated in both *TP53* (H214R substitution associated with second allele loss) [15] and *CTNNB1* (S45A substitution associated with second allele loss, Cavard C., personal communication).

Metabolic reprogramming gives hepatic cancer cells the ability to adapt to energy requirements and environmental constraints. To avoid oxidative stress, cancer cells can either develop a proficient ROS scavenging system or undergo metabolic reprogramming to curb ROS production. Notably, a glycolytic phenotype may allow cells to produce enough energy to maintain their functions while reducing ROS production and oxidative damage [52–54]. In this work, we show that hepatic CSCs exhibit reduced mitochondrial biogenesis and harbor a mitochondrial network with fewer branching points than differentiated tumor-derived hepatocytes. Such a fragmented network, which we have shown to be linked to PPARG expression in HepaRG-CSCs, would favor the adoption of a glycolytic profile and self-renewal properties of stem cells rather than commitment in cell differentiation [55]. Unlike stem cells that produce antioxidants and/or express antioxidant enzymes [53], HepaRG-CSCs express low levels of antioxidant enzymes [11]. As a result, recovery of mitochondrial respiration by silencing *PPARG* and/or inhibiting its target gene *PDK4* leads to increased ROS production and cell death in both HepaRG- and BC2-spheres. Indeed, PDK4-induced metabolic shift is beneficial for CSCs because it limits the production of mitochondrial ROS that can oxidatively damage lipids, proteins and nucleic acids, especially when cellular antioxidant defenses are overwhelmed [54]. In addition, PDK4 could restrain ferroptosis by limiting iron-dependent phospholipid peroxidation that mainly occurs when the TCA cycle is functional [56]. Therefore, glycolytic reprogramming and high expression of PPARG/PDK4 in retrodifferentiated-derived hepatic CSCs contribute to limiting ROS production and the resulting damages.

Besides a glycolytic phenotype, hepatic CSCs also exhibit an altered lipid metabolism that may help prevent oxidative damage. Hepatic CSCs store more saturated than unsaturated lipids, the latter being prone to peroxidative attack [57]. Thus, high levels of saturated FAs are thought to decrease lipid peroxidation and subsequent ROS-induced damage by diluting polyunsaturated FAs in cell membranes [58]. Both low de novo lipogenesis and desaturase activity probably explain the low level of unsaturated lipids in hepatic CSCs. Low de novo lipogenesis might also force hepatic CSCs to use extracellular FAs, in particular through increased expression of the membrane transporter FAT/CD36. Once taken up, lipids are not shuttled into mitochondria to produce energy, but rather stored in droplets. In consistency with these observations, the accumulation of lipid droplets has been associated with stemness in various cancer types [59–61]. By sequestrating lipids, the droplet core provides a protective environment limiting lipid oxidation and oxidative stress [62]. In addition, lipid storage likely provides a source of energy that can be quickly mobilized to meet energy

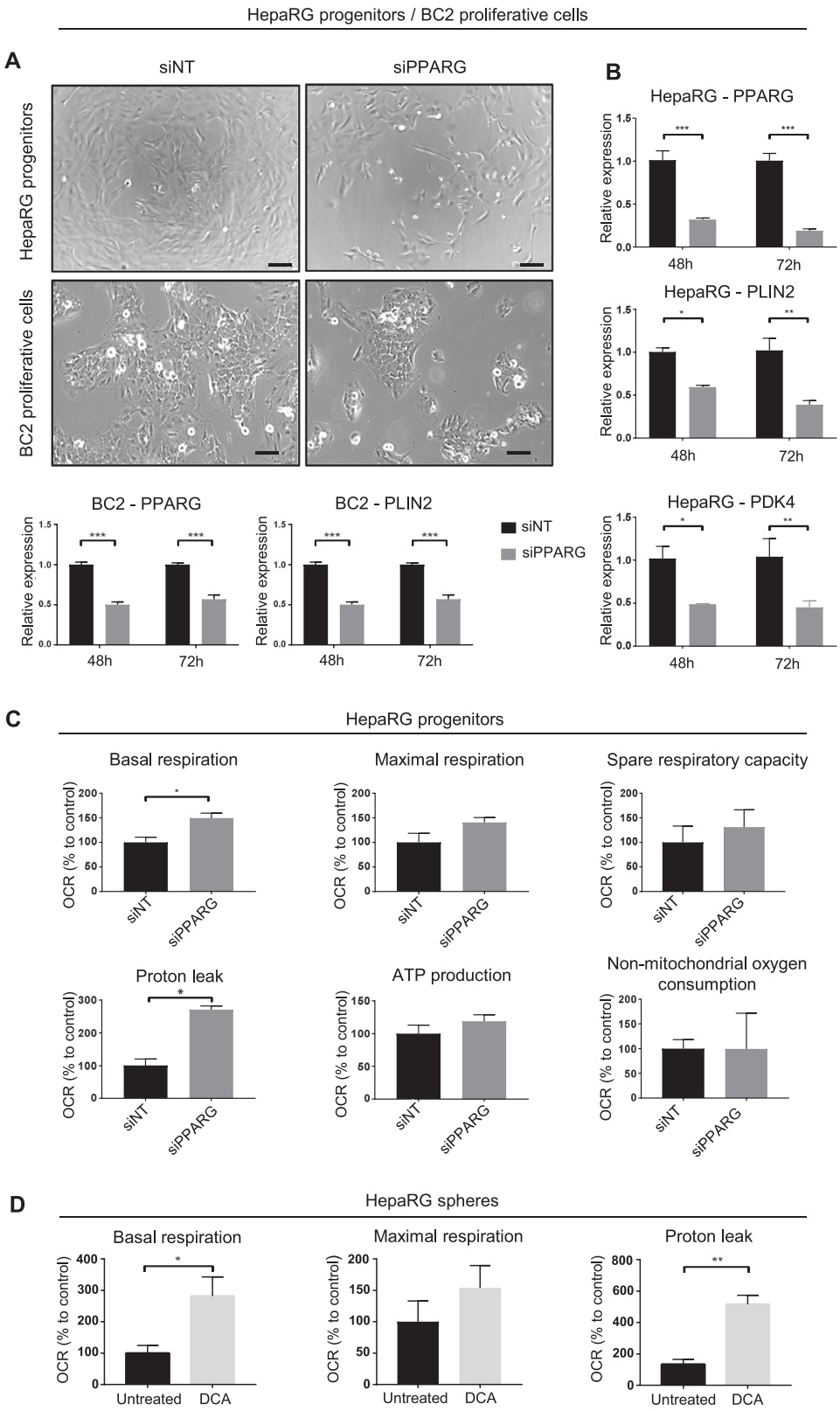

Fig. 6 PPARγ inhibition reduces PDK4 and PLIN2 expression and restores respiration. A Phase-contrast microscopy of HepaRG-progenitors and BC2-proliferative cells 48 h after transfection with si*PPARG*. Bar = 100 µm. **B** mRNA expression of *PPARG*, *PLIN2* and *PDK4*, 48 h and 72 h after transfection of si*PPARG* in HepaRG-progenitors and BC2-proliferative cells ($n = 3$). **C** Basal respiration, maximal respiration, spare respiratory capacity, proton leak, respiration linked to ATP production and non-mitochondrial oxygen consumption, assessed with Seahorse analyzer in HepaRG-progenitors, 48 h after transfection of si*PPARG* ($n = 3$). Results are expressed relative to siNT. **D** Basal respiration, maximal respiration and proton leak assessed with Seahorse analyzer in HepaRG-spheres treated by DCA (50 mM) during 4 h. Results are expressed relative to untreated HepaRG-spheres ($n \geq 3$). *$p < 0.05$, **$p < 0.01$, ***$p < 0.001$.

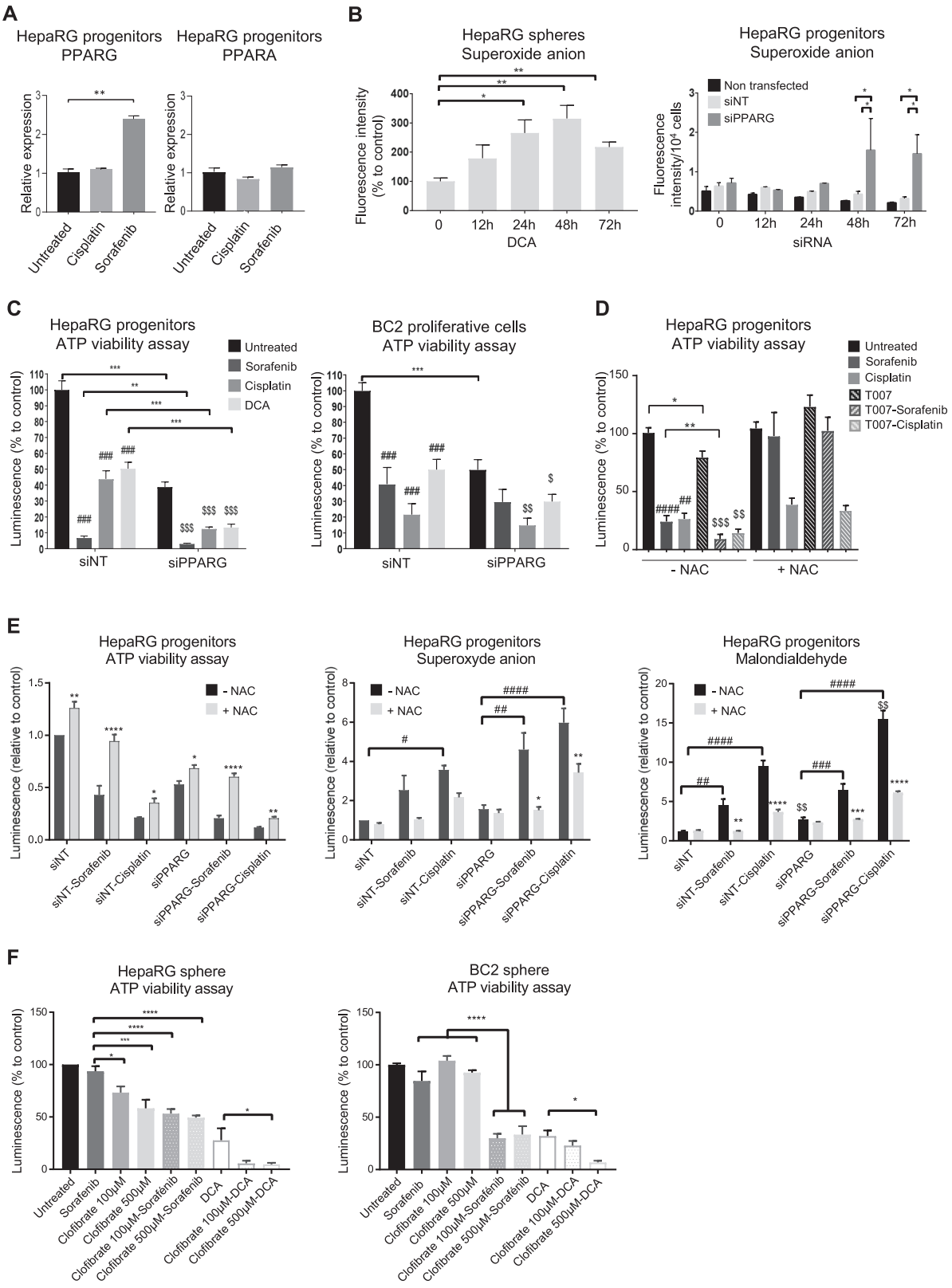

requirements during cell proliferation or differentiation. Accordingly, decreased lipid content is concomitant with the restoration of FAO in proliferating and differentiating HepaRG cells. Furthermore, HepaRG-spheres are arrested in G1 phase of the cell cycle and harbor more lipid droplets than HepaRG-SP [11], which express a higher level of the S and M phase markers. Interestingly, the phenotype of HepaRG-SP displays similarities with hepatic tumor-initiating stem-like cells described by Chen et al. [52], which have self-renewal ability, low OXPHOS, but active FAO. Of note, the pluripotency transcription factor NANOG that

Fig. 7 PPARγ inhibition or agonist-mediated activation of PPARα improves the efficacy of standard HCC chemotherapies in vitro. **A** *PPARG* and *PPARA* expression in HepaRG progenitors after treatment during 72 h with cisplatin (10 µl/ml) or sorafenib (2.5 µM) ($n = 4$) **$p < 001$. **B** Superoxide anion production (ROS) assessed by Mitosox® in HepaRG-spheres after 50 µM dicloroacetate (DCA) treatment during 12 h, 24 h, 48 h and 72 h ($n = 4$) or in HepaRG progenitors after 12 h, 24 h, 48 h and 72 h transfection with si*PPARG* or siNT ($n = 4$). *$p < 0.05$; **$p < 001$. **C** Viability of HepaRG-progenitors and BC2-proliferative cells transfected with si*PPARG* or siNT and treated with cisplatin (10 µg/ml for HepaRG; 20 µg/ml for BC2) or sorafenib (2.5 µM for HepaRG; 15 µM for BC2) or 50 mM DCA during 48 h. Results are expressed relative to untransfected/untreated cells ($n = 4$ for HepaRG and $n = 3$ for BC2). *, #, $ in comparison to siNT, untreated siNT and untreated si*PPARG*, respectively. **D** Viability of HepaRG-progenitors pre-incubated 24 h or not with N-acetyl-cysteine (NAC, 1 mM) and treated during 48 h with cisplatin (10 µg/ml) or sorafenib (2.5 µM) combined or not with T0070907 (10 µM). Results are expressed relative to untreated cells ($n = 3$). *, T0070907 vs untreated; #, cisplatin or sorafenib vs untreated; $, cisplatin or sorafenib vs cisplatin or sorafenib combined with T0070907. **E** Viability, superoxide anion production, lipid peroxidation assessed by malondialdehyde formation in HepaRG transfected with si*PPARG* or siNT, pre-incubated 48 h or not with NAC (1 mM) and treated during 48 h with cisplatin (10 µg/ml) or sorafenib (2.5 µM). *, NAC vs without NAC; #, cisplatin or sorafenib vs untreated; $, siPPARG vs siNT. **F** Viability of HepaRG- and BC2-spheres pre-treated 24 h with clofibrate (100 or 500 µM) and then treated with sorafenib (2.5 µM for HepaRG; 15 µM for BC2) and/or DCA (50 mM) during 72 h. Results are expressed relative to untreated cells ($n = 4$ for HepaRG and $n = 3$ for BC2). *, #, $ $p < 0.05$; **, $$ $p < 0.01$; ***, ###, $$$$p < 0.001$. ****, #### $p < 0.0001$.

represses OXPHOS and mitochondrial ROS production in these hepatic tumor-initiating cells is expressed in HepaRG-CSCs [7, 11]. In addition, HepaRG- and BC2-CSCs express the transcription factor *KLF4*, which drives stemness phenotype during somatic cell reprogramming. KLF4 also favors EPCAM and CD133 expression when overexpressed in Huh7 cells [63]. Thus, the retrodifferentiation process leads differentiated malignant hepatocytes to adopt a CSC-like phenotype characterized by low proliferation rate and energy metabolism, limiting ROS production and lipid storage for future needs.

The nuclear receptors PPARs orchestrate lipid and glucose metabolism, and emerging evidence indicates a complex relationship between PPARs and HCC development. Here, we demonstrate that the differentiation/retrodifferentiation process in HCC cells is modulated by a balanced expression of PPARα/γ isoforms. PPARα, the main isoform expressed in the liver, is found in differentiated tumor-derived hepatocytes, associated with high PGC1α expression, branched mitochondrial network and OXPHOS. High *PPARα* expression is also associated with favorable outcomes in HCCs in two patient datasets (TCGA-LIHC and ICGC). However, the cellular localization of PPARα should be considered with more attention for the stratification within the cohorts because patients with reduced nuclear localization of PPARα have a poorer prognosis [23]. On the other hand, PPARγ, which is not expressed in the basal state in differentiated hepatocytes, is found in steatosis [22] and steatosis-associated liver cancers [28, 30]. Unexpectedly, we found a PPARγ expression in hepatic CSCs. This could result from high AKT signaling and low expression of HNFα1, a crucial transcription factor for hepatocyte differentiation we previously reported in HepaRG-spheres and -SP [11]. Indeed, it was recently shown that AKT2 phosphorylation promotes PPARγ expression through negative regulation of HNF1α [28]. Unlike PPARα, high level of PPARγ is associated with low levels of PGC1α, a fragmented mitochondrial network and negative regulation of numerous genes involved in the TCA cycle and OXPHOS. In line with these observations, the balance *PPARA/PPARG* affects the prognosis of HCCs and high *PPARG* expression is associated with poor overall survival in three independent HCC cohorts (TCGA-LIHC, ICGC and Roessler), totaling 843 patients. Yu et al. [27] previously demonstrated that PPARγ limits HCC cell proliferation and growth. Consistent with this data, our results show that PPARγ activation by the agonist rosiglitazone reduces hepatic CSC proliferation. Importantly, PPARγ-induced metabolic rewiring, associated with the acquisition of stemness features, leads to chemoresistance of HCC cells. These observations are discrepant with a recent work showing that PPARγ is required for PGC1α-induced inhibition of Wnt/βcatenin/PDK1 axis and metastasis in HCCs [26]. This discrepancy might be related to the low expression of PGC1α in hepatic CSCs and/or to the ratio PPARα/PPARγ, which may be different depending on the differentiation state of the cells studied. Interestingly, in line with the deleterious role of PPARγ in HCC, Xiong et al. recently showed that PPARγ signaling promotes resistance to checkpoint inhibitors via induction of VEGFA transcription, which drives an immunosuppressive environment with myeloid-derived suppressor cell expansion and CD8 T cell dysfunction [64]. In agreement with this observation, we previously observed that HepaRG-CSC expressed VEGFA [11]. In summary, our work provides new insights into PPARγ activation in HCC cells. PPARγ 1) induces the expression of the stem cell marker, KLF4, 2) modulates the expression of the EMT markers SNAIL and E-Cadherin, 3) increases the expression of the FA transporter FAT/CD36 and PLIN2, a lipid droplet-stabilizing protein, 4) enhances the expression of PDK4, a pivotal actor of metabolic flexibility and 5) alters the mitochondrial network and respiration capacity. In conclusion, we demonstrate that the balance between PPAR isoforms modulates the metabolic and phenotypic reprogramming in HCC cells. Specifically, PPARγ rewires cell metabolism toward that of stem cells, contributing to chemoresistance. Our work brings out an underestimated function of PPARγ in the process of liver cell differentiation/retrodifferentiation and strengthens the interest in evaluating cell differentiation modulators as new therapeutic options for HCC.

DATA AVAILABILITY

The authors confirm that the data supporting the findings of this study are available within the article and/or its Supplemental Materials and methods. Any additional data are available from the corresponding author upon reasonable request.

REFERENCES

1. Boyault, Rickman S, Reyniès DS, de A, Balabaud C, Rebouissou S, et al. Transcriptome classification of HCC is related to gene alterations and to new therapeutic targets. Hepatology. 2007;45:42–52.
2. Chiang DY, Villanueva A, Hoshida Y, Peix J, Newell P, Minguez B, et al. Focal gains of *VEGFA* and molecular classification of hepatocellular carcinoma. Cancer Res. 2008;68:6779–88.
3. Hoshida Y, Nijman SMB, Kobayashi M, Chan JA, Brunet J-P, Chiang DY, et al. Integrative transcriptome analysis reveals common molecular subclasses of human hepatocellular carcinoma. Cancer Res. 2009;69:7385–92.
4. Lee J-S, Heo J, Libbrecht L, Chu I-S, Kaposi-Novak P, Calvisi DF, et al. A novel prognostic subtype of human hepatocellular carcinoma derived from hepatic progenitor cells. Nat Med. 2006;12:410–6.
5. Thorgeirsson SS. Stemness in liver cancer. Dig Dis. 2017;35:387–9.
6. Theise ND. Hepatic stem cells and cancers: a pathologist's view. Hepat Oncol. 2015;2:329–34.
7. Dubois Pot Schneider H, Fekir K, Coulouarn C, Glaise D, Aninat C, Jarnouen K, et al. Inflammatory cytokines promote the retrodifferentiation of tumor-derived hepatocyte-like cells to progenitor cells. Hepatology. 2014;60:2077–90.
8. Cabillic F, Corlu A. Regulation of transdifferentiation and retrodifferentiation by inflammatory cytokines in hepatocellular carcinoma. Gastroenterology. 2016;151:607–15.
9. Turdo A, Veschi V, Gaggianesi M, Chinnici A, Bianca P, Todaro M, et al. Meeting the challenge of targeting cancer stem cells. Front Cell Dev Biol. 2019;7:16–32.

10. De Francesco EM, Sotgia F, Lisanti MP. Cancer stem cells (CSCs): metabolic strategies for their identification and eradication. Biochem J. 2018;475:1611–34.
11. Fekir K, Dubois-Pot-Schneider H, Désert R, Daniel Y, Glaise D, Rauch C, et al. Retrodifferentiation of human tumor hepatocytes to stem cells leads to metabolic reprogramming and chemoresistance. Cancer Res. 2019;79:1869–83.
12. Yang C, Huang X, Liu Z, Qin W, Wang C. Metabolism-associated molecular classification of hepatocellular carcinoma. Mol Oncol. 2020;14:896–913.
13. Désert R, Rohart F, Canal F, Sicard M, Desille M, Renaud S, et al. Human hepatocellular carcinomas with a periportal phenotype have the lowest potential for early recurrence after curative resection. Hepatology. 2017;66:1502–18.
14. Senni N, Savall M, Granados DC, Alves-Guerra M-C, Sartor C, Lagoutte I, et al. β-catenin-activated hepatocellular carcinomas are addicted to fatty acids. Gut. 2019;68:322–34.
15. Glaise D, Ilyin GP, Loyer P, Cariou S, Bilodeau M, Lucas J, et al. Cell cycle gene regulation in reversibly differentiated new human hepatoma cell lines. Cell Growth Differ. 1998;9:165.
16. Lehrke M, Lazar MA. The many faces of PPARγ. Cell. 2005;123:993–9.
17. Lefterova MI, Zhang Y, Steger DJ, Schupp M, Schug J, Cristancho A, et al. PPARγ and C/EBP factors orchestrate adipocyte biology via adjacent binding on a genome-wide scale. Genes Dev. 2008;22:2941–52.
18. Srivastava N, Kollipara RK, Singh DK, Sudderth J, Hu Z, Nguyen H, et al. Inhibition of cancer cell proliferation by pparγ is mediated by a metabolic switch that increases reactive oxygen species levels. Cell Metab. 2014;20:650–61.
19. Berthier A, Johanns M, Zummo FP, Lefebvre P, Staels B. PPARs in liver physiology. Biochim Biophys Acta Mol Basis Dis. 2021;1867:166097.
20. Desvergne B, Michalik L, Wahli W. Transcriptional regulation of metabolism. Physiol Rev. 2006;86:465–514.
21. Pettersen IKN, Tusubira D, Ashrafi H, Dyrstad SE, Hansen L, Liu X-Z, et al. Upregulated PDK4 expression is a sensitive marker of increased fatty acid oxidation. Mitochondrion. 2019;49:97–110.
22. Mello T, Materozzi M, Galli A. PPARs and mitochondrial metabolism: from NAFLD to HCC. PPAR Res. 2016;2016:e7403230.
23. Xiao Y, Cai S, Liu L, Yang X, Yun J. Decreased expression of peroxisome proliferator-activated receptor alpha indicates unfavorable outcomes in hepatocellular carcinoma. Cancer Manag Res. 2018;10:1781–9.
24. Shen B, Chu ESH, Zhao G, Man K, Wu C-W, Cheng JTY, et al. PPARgamma inhibits hepatocellular carcinoma metastases in vitro and in mice. Br J Cancer. 2012;106:1486–94.
25. To JC, Chiu AP, Tschida BR, Lo LH, Chiu CH, Li X-X, et al. ZBTB20 regulates WNT/CTNNB1 signalling pathway by suppressing PPARG during hepatocellular carcinoma tumourigenesis. JHEP Rep. 2020;3:100223–2233.
26. Zuo Q, He J, Zhang S, Wang H, Jin G, Jin H, et al. PPARγ coactivator-1α suppresses metastasis of hepatocellular carcinoma by inhibiting warburg effect by PPARγ–dependent WNT/β-catenin/pyruvate dehydrogenase kinase isozyme 1 axis. Hepatology. 2021;73:644–60.
27. Yu J, Qiao L, Zimmermann L, Ebert MPA, Zhang H, Lin W, et al. Troglitazone inhibits tumor growth in hepatocellular carcinoma in vitro and in vivo. Hepatology. 2006;43:134–43.
28. Patitucci C, Couchy G, Bagattin A, Cañeque T, de Reyniès A, Scoazec J-Y, et al. Hepatocyte nuclear factor 1α suppresses steatosis-associated liver cancer by inhibiting PPARγ transcription. J Clin Invest. 2017;127:1873–88.
29. Schaefer KL, Wada K, Takahashi H, Matsuhashi N, Ohnishi S, Wolfe MM, et al. Peroxisome proliferator-activated receptor γ inhibition prevents adhesion to the extracellular matrix and induces anoikis in hepatocellular carcinoma cells. Cancer Res. 2005;65:2251–9.
30. Ning Z, Guo X, Liu X, Lu C, Wang A, Wang X, et al. USP22 regulates lipidome accumulation by stabilizing PPARγ in hepatocellular carcinoma. Nat Commun. 2022;13:2187.
31. Wagner N, Wagner K-D. Peroxisome proliferator-activated receptors and the hallmarks of cancer. Cells. 2022;11:2432.
32. Esmaeili S, Salari S, Kaveh V, Ghaffari SH, Bashash D. Alteration of PPARγ) and PTEN gene expression in acute myeloid leukemia patients and the promising anticancer effects of PPARγ stimulation using pioglitazone on AML cells. Mol Genet Genom Med. 2021;9:e1818
33. Lin S-J, Yang D-R, Wang N, Jiang M, Miyamoto H, Li G, et al. TR4 nuclear receptor enhances prostate cancer initiation via altering the stem cell population and EMT signals in the PPARG-deleted prostate cells. Oncoscience. 2015;2:142–50.
34. Moon CM, Kwon J-H, Kim JS, Oh S-H, Jin Lee K, Park JJ, et al. Nonsteroidal anti-inflammatory drugs suppress cancer stem cells via inhibiting PTGS2 (cyclooxygenase 2) and NOTCH/HES1 and activating PPARG in colorectal cancer. Int J Cancer. 2014;134:519–29.
35. Wang X, Sun Y, Wong J, Conklin DS. PPARγ maintains ERBB2-positive breast cancer stem cells. Oncogene. 2013;32:5512–21.
36. Han E, Jang S-Y, Kim G, Lee Y, Choe EY, Nam CM, et al. Rosiglitazone use and the risk of bladder cancer in patients with type 2 diabetes. Medicine. 2016;95:e2786.
37. Taub M. Cancer drug troglitazone stimulates the growth and response of renal cells to hypoxia inducible factors. Biochem Biophys Res Commun. 2016;471:342–7.
38. Cerec V, Glaise D, Garnier D, Morosan S, Turlin B, Drenou B, et al. Transdifferentiation of hepatocyte-like cells from the human hepatoma HepaRG cell line through bipotent progenitor. Hepatology. 2007;45:957–67.
39. Yang L, Wang W-H, Qiu W-L, Guo Z, Bi E, Xu C-R. A single-cell transcriptomic analysis reveals precise pathways and regulatory mechanisms underlying hepatoblast differentiation. Hepatology. 2017;66:1387–401.
40. Li T, Huang J, Jiang Y, Zeng Y, He F, Zhang MQ, et al. Multi-stage analysis of gene expression and transcription regulation in C57/B6 mouse liver development. Genomics. 2009;93:235–42.
41. Gripon P, Rumin S, Urban S, Seyec JL, Glaise D, Cannie I, et al. Infection of a human hepatoma cell line by hepatitis B virus. Proc Natl Acad Sci. 2002;99:15655–60.
42. Coste A, de L, Romagnolo B, Billuart P, Renard C-A, et al. Somatic mutations of the β-catenin gene are frequent in mouse and human hepatocellular carcinomas. Proc Natl Acad Sci. 1998;95:8847–51.
43. Allard J, Bucher S, Massart J, Ferron P-J, Le Guillou D, Loyant R, et al. Drug-induced hepatic steatosis in absence of severe mitochondrial dysfunction in HepaRG cells: proof of multiple mechanism-based toxicity. Cell Biol Toxicol. 2021;37:151–75.
44. Byrne FL, Poon IKH, Modesitt SC, Tomsig JL, Chow JDY, Healy ME, et al. Metabolic vulnerabilities in endometrial cancer. Cancer Res. 2014;74:5832–45.
45. Calvo SE, Clauser KR, Mootha VK. MitoCarta2.0: an updated inventory of mammalian mitochondrial proteins. Nucleic Acids Res. 2016;44:D1251–D1257.
46. Rossignol R, Gilkerson R, Aggeler R, Yamagata K, Remington SJ, Capaldi RA. Energy substrate modulates mitochondrial structure and oxidative capacity in cancer cells. Cancer Res. 2004;64:985–93.
47. Wurmbach E, Chen YB, Khitrov G, Zhang W, Roayaie S, Schwartz M, et al. Genome-wide molecular profiles of HCV-induced dysplasia and hepatocellular carcinoma. Hepatology. 2007;45:938–47.
48. Kaposi-Novak P, Libbrecht L, Woo HG, Lee YH, Sears NC, Coulouarn C, et al. Central role of c-Myc during malignant conversion in human hepatocarcinogenesis. Cancer Res. 2009;69(Apr):2775–82.
49. Ally A, Balasundaram M, Carlsen R, Chuah E, Clarke A, Dhalla N, et al. Comprehensive and integrative genomic characterization of hepatocellular carcinoma. Cell. 2017;169:1327–41.e23.
50. Roessler S, Jia H-L, Budhu A, Forgues M, Ye Q-H, Lee J-S, et al. A unique metastasis gene signature enables prediction of tumor relapse in early-stage hepatocellular carcinoma patients. Cancer Res. 2010;70:10202–12.
51. Nault JC, Mallet M, Pilati C, Calderaro J, Bioulac-Sage P, Laurent C, et al. High frequency of telomerase reverse-transcriptase promoter somatic mutations in hepatocellular carcinoma and preneoplastic lesions. Nat Commun. 2013;4:2218.
52. Chen C-L, Uthaya Kumar DB, Punj V, Xu J, Sher L, Tahara SM, et al. NANOG metabolically reprograms tumor-initiating stem-like cells through tumorigenic changes in oxidative phosphorylation and fatty acid metabolism. Cell Metab. 2016;23:206–19.
53. Kobayashi CI, Suda T. Regulation of reactive oxygen species in stem cells and cancer stem cells. J Cell Physiol. 2012;227:421–30.
54. Ghanbari Movahed Z, Rastegari-Pouyani M, Mohammadi Mhossein, Mansouri K. Cancer cells change their glucose metabolism to overcome increased ROS: one step from cancer cell to cancer stem cell?. Biomed Pharmacother. 2019;112:108690.
55. Chen H, Chan DC. Mitochondrial dynamics in regulating the unique phenotypes of cancer and stem cells. Cell Metab. 2017;26:39–48.
56. Song X, Liu J, Kuang F, Chen X, Zeh HJ, Kang R, et al. PDK4 dictates metabolic resistance to ferroptosis by suppressing pyruvate oxidation and fatty acid synthesis. Cell Rep. 2021;34:108767–90.
57. Visweswaran M, Arfuso F, Warrier S, Dharmarajan A. Aberrant lipid metabolism as an emerging therapeutic strategy to target cancer stem cells. Stem Cells. 2020;38:6–14.
58. Rysman E, Brusselmans K, Scheys K, Timmermans L, Derua R, Munck S, et al. De novo lipogenesis protects cancer cells from free radicals and chemotherapeutics by promoting membrane lipid saturation. Cancer Res. 2010;70:8117–26.
59. Hershey BJ, Vazzana R, Joppi DL, Havas KM. Lipid droplets define a subpopulation of breast cancer stem cells. J Clin Med. 2020;9:87.
60. Tirinato L, Liberale C, Di Franco S, Candeloro P, Benfante A, La Rocca R, et al. Lipid droplets: a new player in colorectal cancer stem cells unveiled by spectroscopic imaging. Stem Cells. 2015;33:35–44.
61. Li J, Condello S, Thomes-Pepin J, Ma X, Xia Y, Hurley TD, et al. Lipid desaturation is a metabolic marker and therapeutic target of ovarian cancer stem cells. Cell Stem Cell. 2017;20:303–14.e5.
62. Bailey AP, Koster G, Guillermier C, Hirst EMA, MacRae JI, Lechene CP, et al. Antioxidant role for lipid droplets in a stem cell niche of Drosophila. Cell. 2015;163:340–53.

63. Firtina Karagonlar Z, Akbari S, Karabicici M, Sahin E, Tercan Avci S, Ersoy N, et al. A novel function for KLF4 in modulating the de-differentiation of EpCAM −/CD133− nonstem cells into EpCAM+/CD133+ liver cancer stem cells in HCC cell line HuH7. Cells. 2020;9:1198.
64. Xiong Z, Chan SL, Zhou J, Vong JSL, Kwong TT, Zeng X, et al. Targeting PPAR-gamma counteracts tumour adaptation to immune-checkpoint blockade in hepatocellular carcinoma. Gut. 2023;72:1758–73.

ACKNOWLEDGEMENTS

The authors thank Pr. Béatrice Desvergne, Faculty of Biology and Medicine, Center for Integrative Genomics, University of Lausanne, for critical reading of the manuscript; Dr Guilia. Bertolin for her advice during the mitochondrial network analysis; Drs. Mireille Desille and Bruno Turlin, CRB-Santé, UAR Biosit, Biogenouest, Rennes, France for tissue bank management; Pascale Bellaud (H2P2 platform, University Rennes 1, Rennes, France); Isabelle Cannie for technical support; Tyéfenn Bouvron, for pre-processing of publicly available raw RNAseq data from mouse liver development models and Patricia Jouas, Adina Pascu and Thomas Poussou for secretarial and informatics support. The authors also thank the "Génomique Santé", "ImPACcell", "flow cytometry", "H2P2" Core facilities from Biogenouest, UAR Biosit, University of Rennes.

AUTHOR CONTRIBUTIONS

AC and FC conceived the study, supervised the work and analyzed the data. YD, LM, SP, CR, KF, LC, LD, DC, AB, CS, CR, TLC performed the experiments and analyzed the data. CA, CB, BC, CA, VR, OM and BF analyzed the data. YD, FC, and AC wrote the manuscript.

FUNDING

The present study was supported by the Institut National de la Santé et de la Recherche Médicale (INSERM), the Centre National de la Recherche Scientifique (CNRS), the University of Rennes, the « Ligue contre le cancer - Comités d'Ille-et-Vilaine, des Côtes d'Armor, de Loire Atlantique, de Vendée, de Charente-Maritime et de la Vienne », Institut National du Cancer (Grant no. 12688) and the European Union's Horizon 2020 Research and Innovation Program, (grant agreement GOLIATH No. 825489).

COMPETING INTERESTS

The authors declare no competing interests.

ETHICS APPROVAL

Human tissue samples were processed by the Biological Resource Center, Rennes University Hospital (BB-0033-00056) after sample examination by the Anatomic Pathology laboratory. The study protocol complied with French laws and regulations and was approved by INSERM's Institutional Review Board (number 19-630) in the context of the National Network of Liver Biological Resource Centers. Sample collection was reported to the Ministry of Education and Research (no. DC-2008-338). All the patients provided written informed consent.

ADDITIONAL INFORMATION

Supplementary information The online version contains supplementary material available at https://doi.org/10.1038/s41419-025-07799-3.

Correspondence and requests for materials should be addressed to Florian Cabillic or Anne Corlu.

Reprints and permission information is available at http://www.nature.com/reprints

Publisher's note Springer Nature remains neutral with regard to jurisdictional claims in published maps and institutional affiliations.